Published in final edited form as:
J Mol Cell Cardiol. 2010 February ; 48(2): 367. doi:10.1016/j.yjmcc.2009.11.003.

Cardiac Overexpression of Metallothionein Rescues Cardiac Contractile Dysfunction and Endoplasmic Reticulum Stress But Not Autophagy in Sepsis

Asli F. Ceylan-Isik[1,*], **Peng Zhao**[1,2,*], **Bingfang Zhang**[3], **Xiaoyan Xiao**[4], **Guohai Su**[5], and **Jun Ren**[1]

[1]Center for Cardiovascular Research and Alternative Medicine, University of Wyoming College of Health Sciences, Laramie, WY 82071 USA

[2]Department of Cardiology, Shandong Provincial Hospital, Shandong University, Jinan 250021, China

[3]Department of Geriatrics, Xijing Hospital, Fourth Military Medical University, Xi'an, China 710032

[4]Department of Endocrinology, Qilu Hospital, Shandong University, Jinan 250012, China

[5]Department of Cardiology, Jinan Central Hospital, Shandong University, Jinan 250013, China

Abstract

Sepsis is characterized by systematic inflammation where oxidative damage plays a key role in organ failure. This study was designed to examine the impact of the antioxidant metallothionein (MT) on lipopolysaccharide (LPS)-induced cardiac contractile and intracellular Ca^{2+} dysfunction, oxidative stress, endoplasmic reticulum (ER) stress and autophagy. Mechanical and intracellular Ca^{2+} properties were examined in hearts from FVB and cardiac-specific MT overexpression mice treated with LPS. Oxidative stress, activation of mitogen-activated protein kinase pathways (ERK, JNK and p38), ER stress, autophagy and inflammatory markers iNOS and TNFα were evaluated. Our data revealed enlarged end systolic diameter, decreased fractional shortening, myocyte peak shortening and maximal velocity of shortening/relengthening as well as prolonged duration of relengthening in LPS-treated FVB mice associated with reduced intracellular Ca^{2+} release and decay. LPS treatment promoted oxidative stress (reduced glutathione/glutathione disulfide ratio and ROS generation). Western blot analysis revealed greater iNOS and TNFα, activation of ERK, JNK and p38, upregulation of ER stress markers GRP78, Gadd153, PERK and IRE1α, as well as the autophagy markers Beclin-1, LCB3 and Atg7 in LPS-treated mouse hearts without any change in total ERK, JNK and p38. Interestingly, these LPS-induced changes in echocardiographic, cardiomyocyte mechanical and intracellular Ca^{2+} properties, ROS, stress signaling and ER stress (but not autophagy, iNOS and TNFα) were ablated by MT. Antioxidant N-acetylcysteine and the ER stress inhibitor tauroursodeoxycholic acid reversed LPS-elicited depression in cardiomyocyte contractile function.

Correspondence should be addressed to: Dr. Jun Ren, Center for Cardiovascular Research and Alternative Medicine, University of Wyoming College of Health Sciences, Laramie, WY 82071, USA Tel: (307) 766-6131; Fax: (307) 766-2953; jren@uwyo.edu.
*These authors contributed equally to this work

DISCLOSURES
None

LPS activated AMPK and its downstream signaling ACC in conjunction with an elevated AMP/ATP ratio, which was unaffected by MT. Taken together, our data favor a beneficial effect of MT in the management of cardiac dysfunction in sepsis.

Keywords

metallothionein; sepsis; cardiomyocytes; oxidative stress; ER stress; autophagy

INTRODUCTION

Sepsis, a major medical problem often leading to multiple organ failure, is one of the main causes of death in critical care medicine (1;2). Among all afflicted organs, heart failure is perhaps the most devastating organ anomaly in septic shock, which contributes to reduced systemic oxygen delivery *en route* to the ultimate multiple organ failure and death (3). Impaired cardiac function is usually the most predominant clinical presentation in septic patients manifested as biventricular dilatation, decreased ejection fraction and myocardial contractility, as well as severe systemic vasodilation with decreased response to fluid resuscitation (4–6). It is widely accepted that the pathogenesis of sepsis is triggered by toxic components of the invading microorganisms including endotoxin from the Gram-negative bacteria lipopolysaccharide (LPS), resulting in systemic disruption of normal inflammatory response (7;8). Nonetheless, the jury is still out with regards to the precise mechanistic processes involved in the progression to organ failure, which has largely hindered the rational therapeutic approaches for sepsis (3).

Up-to-date, activation of multiple stress signaling cascades such as inducible nitric oxide synthase (iNOS), oxidative stress and mitogen-activated protein kinase (MAPK) are believed to play a pivotal role in the pathogenesis of septic cardiac dysfunction (3;9–11). This notion has received convincing supports from the beneficial effects of antioxidants, free radical scavengers and peroxisome proliferator-activated receptor (PPAR)-α agonists against sepsis (12;13). Recent evidence also depicted a role of disrupted mitochondrial ATP production due to mitochondrial oxidative damage, which may serve as a major cause of cell death and organ failure in sepsis (14;15). Moreover, profound oxidative stress was reported in septic patients, and is manifested by elevated lipid peroxides and circulating free radicals, reduced antioxidant capacity, generation of redox-reactive iron, activation of xanthine oxidase and poor handling of exogenous antioxidants (16–18) Furthermore, a deranged mitochondrial redox state has been described in septic patients and experimental sepsis (14;19). Nonetheless, whether oxidative damage is a central pathological mechanism in sepsis-induced organ failure is still controversial since no conclusive evidence is available with regards to the beneficial effect of antioxidant in critically ill patients (20). Recently, *N*-acetylcysteine and the mitochondria-targeted antioxidant MitoQ were demonstrated to reconcile oxidative damage and mitochondrial dysfunction in multiple organs including liver and kidney in experimental models of sepsis (14;21;21). However, little information is available with regards to the impact of antioxidant on cardiac dysfunction in sepsis. More recent evidence from our group indicated a beneficial role of insulin-like growth factor I (IGF-1) in rescuing cardiac contractile dysfunction in sepsis (22). Therefore, the present study was designed to examine the effect of metallothionein (MT), a low molecular weight heavy metal chelating antioxidant, on LPS-induced septic cardiac dysfunction and oxidative damage. Recent data have implicated the cardioprotective properties of MT against diabetes mellitus-, obesity- and aging-induced cardiac damage (23;24). Echocardiographic, cardiomyocyte contractile and intracellular Ca^{2+} properties, accumulation of reactive oxygen species (ROS), oxidative stress, proinflammatory markers (iNOS and TNFα) and MAPK stress signaling cascades [extracellular signal related kinase (ERK), c-jun N-terminal kinase (JNK) and p38] were evaluated in adult wild-type FVB and transgenic mice

with cardiac-specific overexpression of MT treated with or without LPS. Given that endoplasmic reticulum (ER) stress and autophagy are closely associated with septic shock (25;26), protein markers of ER stress [GRP78, Gadd153, protein kinase RNA (PKR)-like ER kinase (PERK), eukaryotic initiation factor 2α (eIF2α) and inositol-requiring protein-1α (IRE1α)] and autophagy [Beclin-1, microtubule-associated protein-1 light chain-3β (LC3B) and Atg7] were also monitored in myocardium of MT transgenic and FVB mice with or without LPS challenge. Levels of AMP and ATP as well as activation of the cellular fuel sensor AMP-activated protein kinase (AMPK) were assessed since sepsis is known to interrupt mitochondrial ATP production in response to mitochondrial oxidative damage (14;15). Last but not the least, lysosomal membrane stability was evaluated in MT and FVB mice following LPS treatment as MT may preserve cell survival and function through protection against oxidative stress-induced lysosomal destabilization (27).

MATERIALS AND METHODS

Experimental animals and LPS treatment

All animal procedures were approved by the Animal Care and Use Committee at the University of Wyoming (Laramie, WY, USA). In brief, adult male mice (5–6 months of age) with a 10-fold transgenic overexpression of MT in the hearts driven by the cardiac-specific mouse α-MHC promoter were used (28). Age- and sex-matched albino FVB mice were used as the wild-type control. All animals were kept in our institutional animal facility with free access to laboratory chow and tap water. On the day of experimentation, both FVB and MT transgenic mice were injected intraperitoneally with 4 or 40 mg/kg *Escherichia Coli O55:B5* LPS (unless otherwise specified in LD_{50} determination) dissolved in sterile saline or an equivalent volume of pathogen-free saline (for control groups). The dosages of LPS injection were chosen based on earlier report of overt myocardial dysfunction without significant mortality (22;29). Four hrs following LPS challenge, mice were sacrificed for experimentation.

Echocardiographic assessment

Cardiac geometry and function were evaluated in anesthetized (Avertin 2.5%, 10 μl/g body weight, i.p.) mice using the 2-D guided M-mode echocardiography (Sonos 5500) equipped with a 15-6 MHz linear transducer. Left ventricular (LV) anterior and posterior wall dimensions during diastole and systole were recorded from three consecutive cycles in M-mode using methods adopted by the American Society of Echocardiography. Fractional shortening was calculated from LV end-diastolic (EDD) and end-systolic (ESD) diameters using the equation (EDD-ESD)/EDD. Estimated echocardiographic LV mass was calculated as (LVEDD + septal wall thickness + posterior wall thickness)^3 − LVEDD^3) × 1.055, where 1.055 (mg/mm^3) is the density of myocardium. Heart rates were averaged over 10 cardiac cycles (24).

Median lethal dose (LD_{50}) of LPS

Adult male FVB and MT mice (5–6 months of age) were each randomly divided into 5 groups (6 mice per group) and were given a single i.p. injection of LPS (8, 17, 25, 33 and 50 mg/kg body weight). Mortality was monitored over a period of 72 hrs. LD_{50} was calculated using the probit analysis method using a BioStat 2008 software (30).

Lysosomal membrane stability

Hearts were rinsed in ice-cold PBS to remove blood contaminants before a portion of the hearts was homogenized in 0.25 ml/l sucrose solution at 4°C. A portion of the homogenate was centrifuged at 600 ×*g* for 10 min at 4°C. The sediment, which contains nuclei, unbroken cells and plasma membrane (nuclear fraction), was suspended in 0.1 M acetate buffer (pH 5.0) prepared in 0.25 M sucrose solution. The supernatant was then centrifuged at 16.000 ×g for

30 min at 4°C before sediment (lysosomal fraction) and supernatant (soluble fraction) were collected separately. The lysosomal fraction was used to determine the characteristic lysosomal enzyme β-glucuronidase activity, which was taken as an index of lysosomal membrane stability (31). In brief, the assay mixture contained 0.5 ml of freshly prepared 4 mM *p*-nitrophenyl β-D-glucuronide (final concentration 2 mM) in 0.1 M sodium acetate buffer (pH 5.0). Twenty-five μl of subcellular fraction was made up to 1.0 ml with assay buffer and was incubated at 37°C for 1 hr. The reaction was stopped by adding 3 ml of 0.2 M glycine-NaOH buffer (pH 11.7). The enzyme was added to the controls after adding glycine buffer. The absorbance was measured at 410 nm using a spectrophotometer (Model Spectra Max 190, Molecular Devices Corp, Sunnyvale, CA, USA). The enzyme activity was expressed as μmol *p*-nitrophenol liberated per hr per 100 mg protein for lysosomal fraction (32).

Isolation of murine cardiomyocytes and in vitro drug treatment

Cardiomyocytes were isolated as described previously (22). In brief, mice were anesthetized using ketamine and xylazine (3:5, 1.32 mg/kg). Hearts were rapidly removed and perfused with oxygenated (5% CO_2/95% O_2) Krebs-Henseleit bicarbonate (KHB) buffer containing (in mM) 118 NaCl, 4.7 KCl, 1.25 $CaCl_2$, 1.2 $MgSO_4$, 1.2 KH_2PO_4, 25 $NaHCO_3$, 10 HEPES, and 11.1 glucose. Hearts were then perfused with a Ca^{2+}-free KHB containing Liberase Blendzyme 4 (Hoffmann-La Roche Inc., Indianapolis, IN, USA) for 20 min. After perfusion, left ventricles were removed and minced to disperse cardiomyocytes in Ca^{2+}-free KHB buffer. Extracellular Ca^{2+} was added incrementally back to 1.25 mmol/l. Myocyte yield was ~ 70% which was not affected by either LPS or MT transgene. Only rod-shaped myocytes with clear edges were selected for mechanical and intracellular Ca^{2+} transient studies. Cells were used within 6 hrs of isolation. To directly assess the role of oxidative stress, ER stress and activation of stress signaling in LPS-induced cardiomyocyte dysfunction, murine cardiomyocytes were incubated with LPS (4 μg/ml) at 37°C for 2 hrs in the absence or presence of the antioxidant N-acetylcysteine (NAC, 500 μM), the ER stress inhibitor tauroursodeoxycholic acid (TUDCA, 500 μM), the ERK inhibitor U0126 (1 μM), the JNK inhibitor SP600125 (1 μM), or the p38 MAPK inhibitor SB203580 (1 μM) prior to mechanical function assessment (33).

Cell shortening/relengthening

Mechanical properties of cardiomyocytes were assessed using a SoftEdge MyoCam system (IonOptix Corporation, Milton, MA, USA) (33). In brief, cardiomyocytes were placed in a chamber mounted on the stage of an inverted microscope (Olympus, IX-70) and superfused at 25°C with a buffer containing (in mM): 131 NaCl, 4 KCl, 1 $CaCl_2$, 1 $MgCl_2$, 10 Glucose and 10 HEPES, at pH 7.4. The cells were field stimulated with suprathreshold voltage at a frequency of 0.5 Hz, 3 msec duration, using a pair of platinum wires placed on opposite sides of the chamber and connected to an electrical stimulator (FHC Inc, Brunswick, NE,USA). The myocyte being studied was displayed on a computer monitor using an IonOptix MyoCam camera. An IonOptix SoftEdge software was used to capture changes in cell length during shortening and relengthening. Cell shortening and relengthening were assessed using the following indices: peak shortening (PS), maximal velocities of cell shortening and relengthening (± dL/dt), time-to-PS (TPS), and time-to-90% relengthening (TR_{90}).

Intracellular Ca^{2+} fluorescence measurement

Myocytes were loaded with fura-2/AM (0.5 μM) for 10 min and fluorescence measurements were recorded with a dual-excitation fluorescence photo multiplier system (Ionoptix). Cardiomyocytes were placed on an Olympus IX-70 inverted microscope and imaged through a Fluor 40× oil objective. Cells were exposed to light emitted by a 75 W lamp and passed through either a 360 or a 380 nm filter, while being stimulated to contract at 0.5 Hz. Fluorescence emissions were detected between 480 and 520 nm by a photomultiplier tube after

first illuminating the cells at 360 nm for 0.5 s then at 380 nm for the duration of the recording protocol (333 Hz sampling rate). The 360 nm excitation scan was repeated at the end of the protocol and qualitative changes in intracellular Ca^{2+} concentration were inferred from the ratio of fura-2 fluorescence intensity at two wavelengths (360/380). Fluorescence decay time was assessed as an indication of intracellular Ca^{2+} clearing. Single exponential curve fit was applied to calculate the intracellular Ca^{2+} decay constant (28).

Western blot analysis

Expression of the stress signaling molecules ERK, JNK and p38, the cell fuel AMPK and acetyl-CoA carboxylase (ACC), the ER stress proteins GRP78, Gadd153, PERK, eIF2α and IRE1α, the autophagy markers Beclin-1, LC3B and Atg7 as well as the proinflammatory markers iNOS and TNFα were assessed. In brief, left ventricular tissue was sonicated in a lysis buffer containing (in mmol/l): Tris 10, NaCl 150, EDTA 5, 1% Triton X-100 and protease inhibitor cocktail followed by centrifugation at 12,000× g for 10 min. Equal amount (30 μg) protein and prestained molecular weight marker were separated using the 7%–12% SDS-polyacrylamide gels in a minigel apparatus (Mini-PROTEAN II, Bio-Rad, Hercules, CA, USA), and were then transferred to nitrocellulose membranes (0.2 μm pore size, Bio-Rad). Membranes were blocked for 1 hr in 5% nonfat milk before being rinsed in TBS-T. The membranes were incubated overnight at 4°C with anti-ERK (1:1,000), anti-pERK (Thr202, 1:1,000), anti-JNK (1:1,000), anti-pJNK (Thr183/Ttyr185, 1:1,000), anti-p38 (1:1,000), anti-pp38 (Thr180/Tyr182, 1:1,000), anti-IRE1α (1:1,000), anti-eIF2α (1:1,000), anti-GRP78 (1:1,000), anti-PERK (1:1,000), anti-Gadd153 (1:1,000), anti-AMPK (1:1,000), anti-pAMPK (Thr172, 1:1,000), anti-ACC (1:1,000), anti-pACC (Ser79, 1:1,000), anti-Beclin-1 (1:1,000), anti-Atg7 (1:1,000), anti-LC3B (1:1,000) anti-TNFα, (1:1,000) and anti-iNOS (1:1,000) antibodies. Anti-ERK and anti-pERK antibodies were purchased from Santa Cruz Biotechnology (Santa Cruz, CA, USA). Anti-pACC and anti-iNOS antibodies were obtained from Upstate Biotechnology (Lake Placid, NY, USA). All other antibodies were acquired from Cell Signaling Technology (Beverly, MA, USA). After incubation with the primary antibodies, blots were incubated with horseradish peroxidase-linked secondary antibodies (1:5,000) for 60 min at room temperature. Immunoreactive bands were detected using the Super Signal West Dura Extended Duration Substrate (Pierce, Milwaukee, WI, USA). The intensity of bands was measured with a scanning densitometer (Model GS-800; Bio-Rad) coupled with a Bio-Rad personal computer analysis software. GAPDH was used as the loading control (28).

Generation of intracellular reactive oxygen species (ROS)

Production of ROS was evaluated by changes in the fluorescence intensity resulted from oxidation of the intracellular fluoroprobe 5- (and -6)-chloromethyl-2′,7′-dichlorodihydrofluorescein diacetate (CM-H_2DCF-DA, Molecular Probes, Eugene, OR,USA). In brief, cardiomyocytes were incubated with 25 μM CM-H_2DCFDA for 30 min at 37°C. Myocytes were then rinsed and the fluorescence intensity was measured using a fluorescent micro-plate reader at the excitation and emission wavelengths of 480 nm and 530 nm, respectively (Molecular Devices, Sunnyvale, CA, USA). Untreated cells without fluorescence were used to determine the background fluorescence. The final results were expressed as the ratio of the fluorescent intensity to respective protein content (28).

Glutathione and glutathione disulfide (GSH/GSSG) assay

The ratio of GSH/GSSG was used as an indicator for oxidative stress. Isolated cardiomyocytes were homogenized in 4 volumes (w/v) of 1% picric acid. Acid homogenates were centrifuged at 13,500 × g (30 min) and supernatant fractions collected. Supernatant fractions were assayed for total GSH and GSSG by the standard recycling method. Half of each sample was used for GSSG determination and the other half was used for GSH. Samples for GSSG determination

were incubated at room temperature with 2 μl of 4-vinyl pyridine (4-VP) per 100 μl sample for 1 hr after vigorous vortexing. Incubation with 4-VP conjugates any GSH present in the sample thus only GSSG is recycled to GSH without potential interference by GSH. The GSSG (as GSH×2) was then subtracted from the total GSH to determine actual GSH level and GSH/GSSG ratio (28).

HPLC assay of AMP/ATP content

The heart tissues were extracted by 6% perchloric acid (Sigma, St. Louis, MO). The acidic homogenate was kept on ice for 30 min, and then centrifuged at 14,000 rpm at 4°C for 10 min. An aliquot of the pellets was set aside for protein measurements. The supernatant was neutralized with 1mol/l K_2CO_3, adjust pH to 3.5. Then kept the supernatant on ice for 10 min and at −80°C for 1–2h to promote precipitation of the perchlorate and centrifuged again. Supernatants were stored at −80°C until HPLC assay. The chromatographic separation of AMP was performed using a Grace Partisil SAX column (250 mm × 4 mm i.d., particle size 10 μm) (Deerfield, IL). The mobile phases were composed of a gradient of 5 mM ammonium dihydrogen phosphate (pH 2.8) and 750 mM ammonium dihydrogen phosphate (pH 3.9). The flow rate was varied from1–2 ml/min over the course of the gradient profile to provide a reasonable assay time of 25 min. The sample injection volume was 50 μl and the components were monitored at 254 nm. The Beckman GOLD HPLC system was operated in laboratory at room temperature (23–25 °C). Concentrations were determined by construction of a calibration curve range from 1 to 80 nmoles per 50 μl injected. Standard stock solutions for calibration curve construction were 6.4 μmole/ml AMP and ATP prepared in 5 mmol/l ammonium dihydrogen phosphate (pH 2.8). These solutions were stored at −80°C and used as references for peaks quantification. Fresh dilution was made before each assay to construct a calibration curve, adding 5 mmol/l ammonium dihydrogen phosphate (pH 2.8) in order to obtain 1, 5, 10, 20, 40 and 80 nmoles per 50 μl injected (34).

Statistical analysis

Data were Mean ± SEM. Difference was assessed using a two-way analysis of variance (ANOVA) followed by a Tukey's *post hoc* test. LD_{50} value was calculated using the probit analysis program with the BioStat2008 software. A p value < 0.05 was considered statistically significant.

RESULTS

General features and echocardiographic properties of FVB and MT mice fed with LPS

LPS treatment did not affect body, liver and kidney weights in either FVB or MT mice. MT transgene did not affect body or organ weights. Heart rate, LV wall thickness, EDD and LV mass (normalized to body weight) were comparable among all groups. LPS significantly increased LV ESD and reduced fractional shortening in FVB hearts, the effect of which was attenuated or ablated by MT transgene. MT transgene did not affect ESD or fractional shortening by itself (Table 1).

Median lethal dose (LD_{50}) of LPS and lysosomal membrane stability

Calculation of LD_{50} exhibited that FVB mice were more susceptible to LPS-induced lethality with a LD_{50} value of 28.89 mg/kg compared with MT mice (LD_{50} = 40.66 mg/kg, $p < 0.05$ *vs*. FVB) within the 72-hr surveillance period (Fig. 1A). Given that MT was reported previously to protect against oxidative stress-induced lysosomal destabilization (27), the characteristic lysosomal enzyme β-glucuronidase activity was evaluated in lysosomal fraction. Our result shown in Fig. 1B indicated neither LPS treatment nor MT transgene affected β-glucuronidase activity, an essential index for lysosomal membrane stability.

Mechanical and intracellular Ca^{2+} properties of murine cardiomyocytes in FVB and MT mice

Neither LPS treatment (both 4 and 40 mg/kg) nor MT transgene affected resting cell length. However, cardiomyocytes from the LPS-treated FVB mice displayed significantly reduced peak shorting (PS) and maximal velocity of shortening/relengthening (±dL/dt) associated with prolonged time-to-90% relengthening (TR_{90}) and normal time-to-PS (TPS). Both doses of LPS elicited comparable changes in cardiomyocyte mechanical function. Interestingly, the antioxidant MT protected the cardiomyocyte mechanical dysfunctions elicited by both low- and high-dosage of LPS without eliciting any overt effect by itself (Fig. 2). To explore the potential mechanism(s) of action involved in the MT-elicited protection against LPS-induced cardiomyocyte contractile dysfunction, intracellular Ca^{2+} homeostasis was evaluated using the fluorescence dye fura-2. Our results indicated that LPS (both 4 and 40 mg/kg) significantly reduced peak intracellular Ca^{2+} and electrically-stimulated rise in intracellular Ca^{2+} as well as prolonged intracellular Ca^{2+} decay rate without affecting the basal intracellular Ca^{2+} levels, the effects of which were nullified by the MT transgene. MT transgene failed to affect intracellular Ca^{2+} properties by itself (Fig. 3).

Effect of MT on LPS-induced ROS generation and oxidative stress

To assess the antioxidant property of MT against LPS-induced endotoxemia in mice, ROS generation and oxidative stress were examined by DCF fluorescence technique and GSH/GSSG assay, respectively. Fig. 4 depicted that LPS treatment (4 mg/kg) greatly facilitated generation of ROS while it reduced the GSH levels as well as the GSH/GSSG ratio in FVB group, consolidating a state of overt oxidative stress. As expected, the heavy metal scavenger MT effectively alleviated the LPS-induced ROS generation and oxidative stress (restored GSH levels and GSH/GSSG ratio).

Effect of MT on LPS-induced activation of stress signaling

LPS challenge is usually associated with activation of stress signaling (35). Results shown in Fig. 5 reveal activation of the stress signaling molecules ERK, JNK, and p38 MAPK in myocardium following LPS treatment (4 mg/kg). While MT itself did not elicit any effect on the phosphorylation status of these signaling molecules, it ablated LPS-induced activation of ERK, JNK and p38. Protein expression of total ERK, JNK and p38 was unaffected by either LPS treatment or MT transgene.

Effect of stress signaling inhibition on LPS-induced cardiomyocyte mechanical dysfunction

To examine if activation of stress signaling molecules contributes to the LPS-induced cardiac contractile defects, freshly isolated cardiomyocytes from wild-type FVB mice were treated with LPS (4 μg/ml) for 2 hrs in the absence or presence of the ERK inhibitor U0126 (1 μM), the JNK inhibitor SP600125 (1 μM) or the p38 MAPK inhibitor SB203580 (1 μM). Similar to the *in vivo* finding, *in vitro* LPS treatment significantly depressed PS and ± dL/dt as well as prolonged TR_{90} without affecting resting cell length and TPS in murine cardiomyocytes. Interestingly, all three kinase inhibitors significantly attenuated or ablated LPS-induced mechanical defects (Fig. 6). None of the kinase inhibitors elicited any significant effects on cardiomyocyte mechanics by themselves (data not shown). This observation provided direct evidence for a role of MAPK stress signaling cascades in the LPS-induced cardiac contractile dysfunction.

Involvement of ER stress and AMPK activation in MT- or LPS-induced cardiac dysfunction

Our result revealed significantly upregulated expression of the ER stress markers GRP78, Gadd153, PERK and IRE1α but not eIF2α in the LPS (4 mg/kg)-treated FVB murine hearts, the effect of which was obliterated by MT. The MT transgene did not affect the expression of GRP78, Gadd153, PERK, eIF2α and IRE1α by itself (Fig. 7). To further consolidate a role of

ER stress in the LPS-induced cardiac contractile defects, freshly isolated FVB cardiomyocytes were treated with LPS (4 μg/ml) for 2 hrs in the absence or presence of the ER stress inhibitor TUDCA (500 μM) or the antioxidant NAC (500 μM) (33). Data shown in Fig. 8 depicted that both TUDCA and NAC effectively reconciled LPS-induced cardiomyocyte mechanical defects (decreased PS and ± dL/dt as well as prolonged TR_{90}) without eliciting any effect by themselves, suggesting direct involvement of both ER stress and oxidative stress in LPS-induced cardiac contractile dysfunction.

Our further study indicated that LPS (4 mg/kg) significantly enhanced the activation of AMPK and its downstream signal ACC, the effect of which was unaffected by MT transgene. MT did not affect the activation of AMPK nor ACC by itself. Neither LPS nor MT significantly affected the expression of total AMPK and ACC (Fig. 9A–B). Consistent with the activation of AMPK and ACC following LPS treatment, AMP levels (data not shown) and the AMP-to-ATP ratio were significantly elevated in response to LPS challenge. Similar to the activation response of AMPK and ACC, MT transgene failed to alter both AMP levels (data not shown) and the AMP-to-ATP ratio (Fig. 9C) under either basal or LPS-challenged condition.

Effect of MT on LPS-induced autophagy and proinflammatory responses

Sepsis is known to be associated with activation of autophagy and proinflammatory response (3;26). To evaluate if autophagy and proinflammatory response play a role in the MT-offered cardioprotection against endotoxemia, protein markers of autophagy (Beclin-1, LC3B and Atg7) and inflammation (iNOS and TNFα) were determined. Data displayed in Fig. 10 reveal upregulation of both autophagy and proinflammatory pathways following LPS treatment (4 mg/kg) evidenced by elevated expression of Beclin-1, LC3B, Atg7, iNOS and TNFα in myocardium, the effects of which were unaffected by the MT transgene. MT did not elicit any effect on these proteins by itself either.

DISCUSSION

Our present study demonstrated that cardiac-specific overexpression of the heavy metal scavenger MT rescued LPS-induced cardiac contractile and intracellular Ca^{2+} dysfunctions. The MT-offered cardioprotection in sepsis may be underscored by alleviation of ROS accumulation, oxidative stress and ER stress. In addition, MT alleviated LPS-induced activation of ERK, JNK and p38 signaling cascades. Our *in vitro* study further consolidated the causative role of oxidative stress, ER stress and stress signaling in LPS-elicited cardiac contractile anomalies. The beneficial myocardial effect of MT was also associated with improved survival and a greater LD_{50} value for LPS in MT mice. Our data did not favor a major role of lysosomal membrane stability, AMP/ATP production, activation of AMPK, autophagy and proinflammatory cascade in the MT-elicited cardioprotection in sepsis. These findings implicate a direct cardiac benefit of antioxidants as opposed to a secondary response of inflammation although the later cannot be fully excluded at this time. Since MT transgene did not alter cardiac geometry and contractile function in the absence of endotoxemia, its beneficial role against LPS-induced cardiac dysfunction, oxidative stress and ER stress entails a therapeutic potential of antioxidants in the clinical management of cardiovascular complication in sepsis.

An ample of clinical and experimental evidence has consolidated the dysregulated cardiac contractile function in sepsis (3;5;35). Our results revealed reduced fractional shortening, PS and ± dL/dt, prolongation of relaxation duration (TR_{90}) in septic hearts, consistent with the previous reports (3;5;22;26;36). The echocardiographic finding of a significantly low fractional shortening in LPS-treated mice is likely attributed to the enlarged end systolic volume (ESD) with unchanged end diastolic volume (EDD), which symbolizes compromised ventricular systolic contractility. The observation that MT alleviated LPS-induced cardiac contractile

dysfunction, intracellular Ca^{2+} dysregulation, ROS accumulation, oxidative stress, activation of stress signaling and ER stress favors a role of improved intracellular Ca^{2+} homeostasis and reduced intracellular ROS accumulation as well as ER stress by the antioxidant MT. The fact that MT failed to alter cardiac geometry, mechanical function and oxidative/ER stress in normal mice suggested that endogenous overexpression of this antioxidant is not innately harmful to the heart. The myocardial benefit of MT in endotoxemia is somewhat consistent with its protective role against cardiac dysfunction in diabetes, obesity and aging (23;24). LPS treatment significantly attenuated electrically-stimulated rise and peak intracellular Ca^{2+}, suggesting an essential role of intracellular Ca^{2+} homeostasis in endotoxemia-induced cardiac dysfunction. Our finding of ablated activation of ERK, JNK and p38 in MT-LPS mice received some convincing support from the kinase inhibitors (U0126, SP600125 and SB203580) and NAC-elicited defense against LPS-induced cardiac contractile defects. These findings are in line with the crucial role of MAPK signaling and oxidative stress in sepsis-induced organ dysfunction including myocardial contractile dysfunction (3;35;37). Involvement of MAPK stress signaling in LPS- and MT-induced myocardial response was further supported by measurement of ROS generation and oxidative stress in these mice.

To-date, the precise role of oxidative damage in the pathogenesis of sepsis-induced heart failure still remains elusive. Although our current study favors a beneficial role of the endogenous antioxidant MT in sepsis-induced cardiac contractile dysfunction and oxidative stress, convincing clinical evidence regarding such beneficial role of antioxidant supplementation in heart failure is lacking (20). One of the possible explanations is that antioxidants are not densely accumulated in mitochondria where they are most required despite the wide distribution of antioxidants throughout the body (14). Recent evidence suggested that archetypal mitochondria-targeted antioxidant MitoQ antagonized sepsis-induced oxidative stress in multiple organs including hearts. The lipophilic triphenylphosphonium cation attached to the ubiquinone antioxidant moiety of the endogenous antioxidant coenzyme Q10 enables MitoQ to be readily taken up through plasma and mitochondrial membranes in the absence of a carrier (14;38). In addition, the huge membrane potential across the mitochondrial inner membrane may help to trap MitoQ in the mitochondria. In consequence, MitoQ is likely several hundredfold more potent in rescuing mitochondrial oxidative stress than an untargeted antioxidant. MT, an intracellular metal-binding proteins with high cysteine contents, may efficiently protect against oxidative damage through suppression of mitochondrial oxidative stress (e.g., mitochondrial GSH depletion) (39). Although it is beyond the scope of our current study, the MT transgene may exert its cardioprotective effect through rescuing mitochondrial oxidative damage. This is in line with the fact that mitochondrial dysfunction contributes directly to impaired cardiac function in sepsis (40). Our data also revealed enhanced AMP/ATP ratio, activation of AMPK and ACC in septic hearts, suggesting an altered energy metabolism and cell fuel status in sepsis. To our surprise, our data did not favor a major role of AMP/ATP production and activation of the cell fuel AMPK in the MT-elicited beneficial effect against cardiac dysfunction and oxidative stress in sepsis. It was reported earlier that little change in the basal high-energy phosphate (i.e., ATP) stores was found in septic canine hearts, despite the overt mitochondrial swelling and impaired contractile function (41). These data suggest that impaired mitochondrial ATP formation may not be a major factor in myocardial contractile dysfunction in sepsis (41). It is plausible to speculate that the heart was already operating at or near maximum capacity in sepsis, thus implying a possible loss of cardiac reserve in sepsis.

ER is an extensive intracellular membranous network involved in Ca^{2+} storage, Ca^{2+} signaling, glycosylation and trafficking of membrane and secretory proteins. Sepsis may perturb these processes in the lung thus creating a condition defined as ER stress (25). Our result revealed overt ER stress in myocardium following LPS-induced endotoxemia. ER stress has been shown to contribute to neurodegenerative disorders, diabetes and ischemia reperfusion-induced heart

damage (42;43). Three distinct classes of ER stress transducers are known namely IRE1, PERK-translation initiation factor eIF-2α pathway and activating transcription factor-6 (ATF6), with each governing a distinct arm of ER stress-induced unfolded protein response (UPR) (43). Our data revealed upregulated ER chaperone GRP78 (also known as BiP) which directly interacts with all three ER stress sensors, PERK/eIF2α, ATF6 and IRE1, under sepsis. Upregulation of GRP78 is pivotal for cell survival to facilitate folding and assembly of ER proteins and prevent them from aggregation during ER stress (43). Our results also depicted upregulation of the UPR pro-apoptotic protein Gadd153, a marker for PERK activity in the UPR (44). Our observation that MT nullified the LPS-induced increase in GRP78, Gadd153, PERK and IRE1α suggests contribution of myocardial ER stress in the antioxidant-elicited beneficial effects in the hearts. The unchanged eIF2α in LPS- and MT-associated responses may be due to the issue of total versus phosphorylated protein expression. Our *in vitro* study using the ER stress inhibitor TUDCA further supported the interplay between ER stress and cardiac dysfunction in septic shock. Our recent data revealed that ER stress directly triggers cardiomyocyte contractile dysfunction (45), consistent with a role of ER stress in sepsis-induced cardiac dysfunction.

Autophagy is a catabolic pathway through which mammalian cells degrade and recycle macromolecules and organelles. Enhanced autophagy in myocardium has been reported in a wide array of cardiovascular diseases including sepsis (26). Autophagy usually starts with an “induction phase” which can be initiated by Beclin-1 as an internal stimulus followed by a second “formation phase” involving Atg proteins such as Atg7 and autophagosomal membrane specific protein light chain 3 (LC3) or Atg8, a marker for autophagosome membrane. Autophagosome fuses with the lysosme before being degraded by lysosomal proteases (46). Data from our present study suggest enhanced autophagy associated with cardiac dysfunction and oxidative stress in septic heart, which is consistent with the notion that autophagy may be upregulated under environmental stress conditions including ATP depletion, reactive oxygen species and mitochondrial dysfunction (46). Paradoxically, recent evidence indicated that autophagy may protect against LPS-associated oxidative stress (47). Our results did not favor a role of autophagy in MT-elicited cardioprotection. Further study is warranted to elucidate the precise role of autophagy in myocardial function in sepsis. Last but not the least, observations from our present study did not favor a major role of lysosomal membrane stability and proinflammatory cascade (such as iNOS and TNFα) in the MT-elicited cardioprotection in sepsis.

In conclusion, our study revealed that the heavy metal scavenger MT rescues LPS-induced cardiac contractile dysfunction and intracellular Ca^{2+} mishandling possibly through alleviation of ROS/oxidative stress, stress signaling activation, and ER stress. The beneficial myocardial effect of MT was associated with improved survival in mice and an increased LD_{50} for LPS. Although more mechanistic scenario remains to be explored such as the role of autophagy, it is becoming apparent that oxidative and ER stress are the main regulatory machineries for cardiac contractile and intracellular Ca^{2+} function under endotoxemia. Nonetheless, the interplay and the sequential relationship between oxidative and ER stress in cardiac and mitochondrial function remains to be determined in the context of sepsis. These approaches should be essential to the application of antioxidants and ER stress inhibitors in the clinical management of endotoxemia-associated cardiac dysfunction.

Acknowledgments

The authors wish to acknowledge Dr. Ji Li and Mr. Machender R. Kandadi from University of Wyoming for their assistance. This work was supported by NIH INBRE P20 RR16474.

Reference List

1. Sprung CL, Annane D, Keh D, Moreno R, Singer M, Freivogel K, et al. Hydrocortisone therapy for patients with septic shock. N Engl J Med 2008;358(2):111–124. [PubMed: 18184957]
2. The outcome of patients with sepsis and septic shock presenting to emergency departments in Australia and New Zealand. Crit Care Resusc 2007;9(1):8–18. [PubMed: 17352661]
3. Ren J, Wu S. A burning issue: do sepsis and systemic inflammatory response syndrome (SIRS) directly contribute to cardiac dysfunction? Front Biosci 2006;11:15–22. [PubMed: 16146710]
4. Bradford SD, Hunter K, Wu Y, Jablonowski C, Bahl JJ, Larson DF. Modulation of the inflammatory response in the cardiomyocyte and macrophage. J Extra Corpor Technol 2001;33(3):167–174. [PubMed: 11680730]
5. Niederbichler AD, Westfall MV, Su GL, Donnerberg J, Usman A, Vogt PM, et al. Cardiomyocyte function after burn injury and lipopolysaccharide exposure: single-cell contraction analysis and cytokine secretion profile. Shock 2006;25(2):176–183. [PubMed: 16525357]
6. Patten M, Kramer E, Bunemann J, Wenck C, Thoenes M, Wieland T, et al. Endotoxin and cytokines alter contractile protein expression in cardiac myocytes in vivo. Pflugers Arch 2001;442(6):920–927. [PubMed: 11680626]
7. Moniotte S, Belge C, Sekkali B, Massion PB, Rozec B, Dessy C, et al. Sepsis is associated with an upregulation of functional beta3 adrenoceptors in the myocardium. Eur J Heart Fail 2007;9(12):1163–1171. [PubMed: 17999941]
8. Neviere RR, Cepinskas G, Madorin WS, Hoque N, Karmazyn M, Sibbald WJ, et al. LPS pretreatment ameliorates peritonitis-induced myocardial inflammation and dysfunction: role of myocytes. Am J Physiol 1999;277(3 Pt 2):H885–H892. [PubMed: 10484407]
9. Cowan DB, Noria S, Stamm C, Garcia LM, Poutias DN, del Nido PJ, et al. Lipopolysaccharide internalization activates endotoxin-dependent signal transduction in cardiomyocytes. Circ Res 2001;88(5):491–498. [PubMed: 11249872]
10. Flesch M, Kilter H, Cremers B, Laufs U, Sudkamp M, Ortmann M, et al. Effects of endotoxin on human myocardial contractility involvement of nitric oxide and peroxynitrite. J Am Coll Cardiol 1999;33(4):1062–1070. [PubMed: 10091837]
11. Gupta A, Sharma AC. Metalloendopeptidase inhibition regulates phosphorylation of p38-mitogen-activated protein kinase and nitric oxide synthase in heart after endotoxemia. Shock 2003;20(4):375–381. [PubMed: 14501953]
12. Zhang WJ, Wei H, Hagen T, Frei B. Alpha-lipoic acid attenuates LPS-induced inflammatory responses by activating the phosphoinositide 3-kinase/Akt signaling pathway. Proc Natl Acad Sci U S A 2007;104(10):4077–4082. [PubMed: 17360480]
13. Jozefowicz E, Brisson H, Rozenberg S, Mebazaa A, Gele P, Callebert J, et al. Activation of peroxisome proliferator-activated receptor-alpha by fenofibrate prevents myocardial dysfunction during endotoxemia in rats. Crit Care Med 2007;35(3):856–863. [PubMed: 17255874]
14. Lowes DA, Thottakam BM, Webster NR, Murphy MP, Galley HF. The mitochondria-targeted antioxidant MitoQ protects against organ damage in a lipopolysaccharide-peptidoglycan model of sepsis. Free Radic Biol Med 2008;45(11):1559–1565. [PubMed: 18845241]
15. Abraham E, Singer M. Mechanisms of sepsis-induced organ dysfunction. Crit Care Med 2007;35(10):2408–2416. [PubMed: 17948334]
16. Goode HF, Cowley HC, Walker BE, Howdle PD, Webster NR. Decreased antioxidant status and increased lipid peroxidation in patients with septic shock and secondary organ dysfunction. Crit Care Med 1995;23(4):646–651. [PubMed: 7712754]
17. Galley HF, Davies MJ, Webster NR. Xanthine oxidase activity and free radical generation in patients with sepsis syndrome. Crit Care Med 1996;24(10):1649–1653. [PubMed: 8874300]
18. Galley HF, Webster NR. Elevated serum bleomycin-detectable iron concentrations in patients with sepsis syndrome. Intensive Care Med 1996;22(3):226–229. [PubMed: 8727436]
19. Yassen KA, Galley HF, Lee A, Webster NR. Mitochondrial redox state in the critically ill. Br J Anaesth 1999;83(2):325–327. [PubMed: 10618950]
20. Mishra V. Oxidative stress and role of antioxidant supplementation in critical illness. Clin Lab 2007;53(3–4):199–209. [PubMed: 17447658]

21. Zapelini PH, Rezin GT, Cardoso MR, Ritter C, Klamt F, Moreira JC, et al. Antioxidant treatment reverses mitochondrial dysfunction in a sepsis animal model. Mitochondrion 2008;8(3):211–218. [PubMed: 18417427]
22. Zhao P, Turdi S, Dong F, Xiao X, Su G, Zhu X, et al. Cardiac-specific overexpression of insulin-like growth factor I (IGF-1) rescues lipopolysaccharide-induced cardiac dysfunction and activation of stress signaling in murine cardiomyocytes. Shock 2009;32(1):100–107. [PubMed: 18948844]
23. Yang X, Doser TA, Fang CX, Nunn JM, Janardhanan R, Zhu M, et al. Metallothionein prolongs survival and antagonizes senescence-associated cardiomyocyte diastolic dysfunction: role of oxidative stress. FASEB J 2006;20(7):1024–1026. [PubMed: 16585059]
24. Dong F, Li Q, Sreejayan N, Nunn JM, Ren J. Metallothionein prevents high-fat diet induced cardiac contractile dysfunction: role of peroxisome proliferator activated receptor gamma coactivator 1alpha and mitochondrial biogenesis. Diabetes 2007;56(9):2201–2212. [PubMed: 17575086]
25. Endo M, Oyadomari S, Suga M, Mori M, Gotoh T. The ER stress pathway involving CHOP is activated in the lungs of LPS-treated mice. J Biochem 2005;138(4):501–507. [PubMed: 16272146]
26. Hsieh YC, Athar M, Chaudry IH. When apoptosis meets autophagy: deciding cell fate after trauma and sepsis. Trends Mol Med 2009;15(3):129–138. [PubMed: 19231289]
27. Baird SK, Kurz T, Brunk UT. Metallothionein protects against oxidative stress-induced lysosomal destabilization. Biochem J 2006;394(Pt 1):275–283. [PubMed: 16236025]
28. Ren J, Privratsky JR, Yang X, Dong F, Carlson EC. Metallothionein alleviates glutathione depletion-induced oxidative cardiomyopathy in murine hearts. Crit Care Med 2008;36(7):2106–2116. [PubMed: 18552690]
29. Peng T, Lu X, Feng Q. Pivotal role of gp91phox-containing NADH oxidase in lipopolysaccharide-induced tumor necrosis factor-alpha expression and myocardial depression. Circulation 2005;111 (13):1637–1644. [PubMed: 15795323]
30. Finney DJ. The adjustment for a natural response rate in probit analysis. Ann Appl Biol 1949;36(2): 187–195. [PubMed: 18151945]
31. Wilson JS, Apte MV, Thomas MC, Haber PS, Pirola RC. Effects of ethanol, acetaldehyde and cholesteryl esters on pancreatic lysosomes. Gut 1992;33(8):1099–1104. [PubMed: 1398235]
32. Koldovsky O. Developmental changes of beta-galactosidase and beta-glucuronidase in the rat liver and kidney. Arch Biochem Biophys 1971;142(1):378–381. [PubMed: 5545489]
33. Guo R, Ma H, Gao F, Zhong L, Ren J. Metallothionein alleviates oxidative stress-induced endoplasmic reticulum stress and myocardial dysfunction. J Mol Cell Cardiol 2009;47(2):228–237. [PubMed: 19344729]
34. Zhao P, Wang J, Ma H, Xiao Y, He L, Tong C, et al. A newly synthetic chromium complex-Chromium (d-phenylalanine)(3) activates AMP-activated protein kinase and stimulates glucose transport. Biochem Pharmacol. 2008
35. Ren J. Wide spectrum of presentation and variable mechanisms of compromised cardiac function in multiple organ dysfunction syndrome. J Organ Dysfunction 2008;4:239–248.
36. Ren J, Ren BH, Sharma AC. Sepsis-induced depressed contractile function of isolated ventricular myocytes is due to altered calcium transient properties. Shock 2002;18(3):285–288. [PubMed: 12353932]
37. Obata T, Brown GE, Yaffe MB. MAP kinase pathways activated by stress: the p38 MAPK pathway. Crit Care Med 2000;28(4 Suppl):N67–N77. [PubMed: 10807318]
38. Murphy MP, Smith RA. Targeting antioxidants to mitochondria by conjugation to lipophilic cations. Annu Rev Pharmacol Toxicol 2007;47:629–656. [PubMed: 17014364]
39. Cai L, Wang Y, Zhou G, Chen T, Song Y, Li X, et al. Attenuation by metallothionein of early cardiac cell death via suppression of mitochondrial oxidative stress results in a prevention of diabetic cardiomyopathy. J Am Coll Cardiol 2006;48(8):1688–1697. [PubMed: 17045908]
40. Joshi MS, Julian MW, Huff JE, Bauer JA, Xia Y, Crouser ED. Calcineurin regulates myocardial function during acute endotoxemia. Am J Respir Crit Care Med 2006;173(9):999–1007. [PubMed: 16424445]
41. Solomon MA, Correa R, Alexander HR, Koev LA, Cobb JP, Kim DK, et al. Myocardial energy metabolism and morphology in a canine model of sepsis. Am J Physiol 1994;266(2 Pt 2):H757–H768. [PubMed: 8141377]

42. Ozcan U, Cao Q, Yilmaz E, Lee AH, Iwakoshi NN, Ozdelen E, et al. Endoplasmic reticulum stress links obesity, insulin action, and type 2 diabetes. Science 2004;306(5695):457–461. [PubMed: 15486293]

43. Ron D, Walter P. Signal integration in the endoplasmic reticulum unfolded protein response. Nat Rev Mol Cell Biol 2007;8(7):519–529. [PubMed: 17565364]

44. Li J, Holbrook NJ. Elevated gadd153/chop expression and enhanced c-Jun N-terminal protein kinase activation sensitizes aged cells to ER stress. Exp Gerontol 2004;39(5):735–744. [PubMed: 15130668]

45. Ren J. Endoplasmic reticulum stress impairs murine cardiomyocyte contractile function via an Akt-dependent mechanism. Circulation 2007;116 II-190 (Abstract).

46. Gustafsson AB, Gottlieb RA. Autophagy in ischemic heart disease. Circ Res 2009;104(2):150–158. [PubMed: 19179668]

47. Hickson-Bick DL, Jones C, Buja LM. Stimulation of mitochondrial biogenesis and autophagy by lipopolysaccharide in the neonatal rat cardiomyocyte protects against programmed cell death. J Mol Cell Cardiol 2008;44(2):411–418. [PubMed: 18062988]

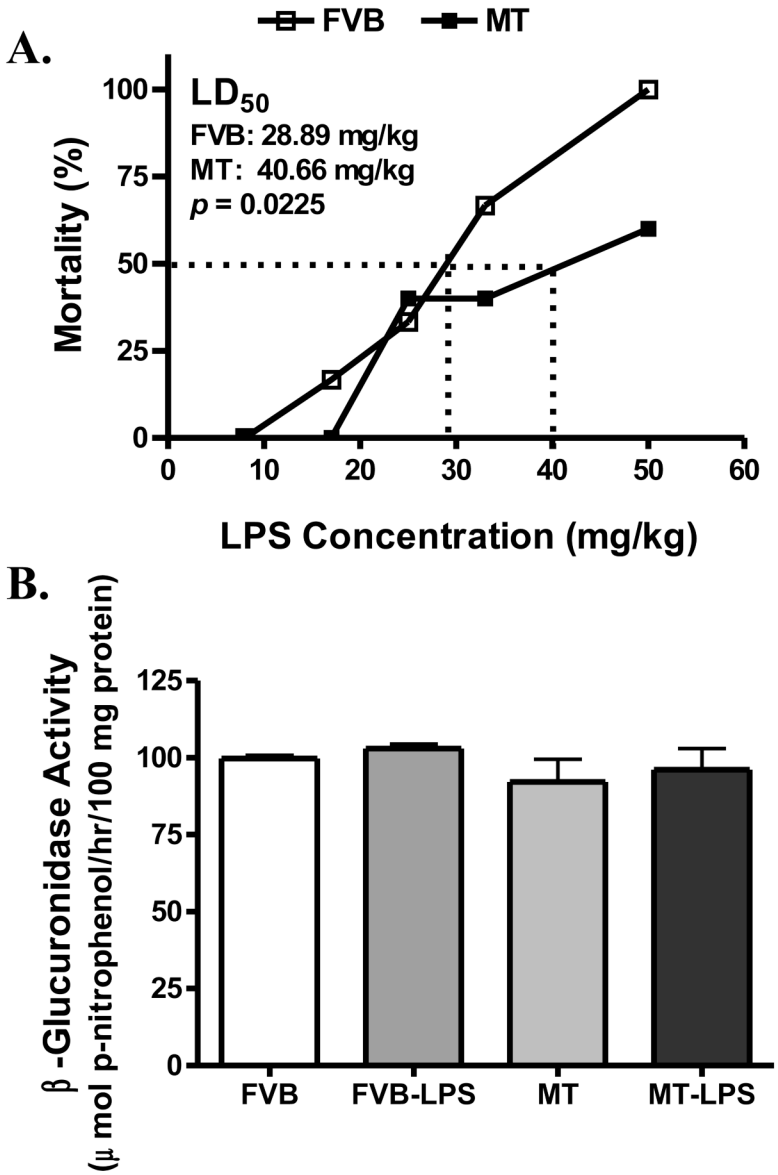

Fig. 1.

Median lethal dose (LD_{50}) and lysosomal membrane stability in FVB and MT mice treated with or without LPS. A: Various dosages of LPS-induced mortality in mice over a period of 72 hrs. LD_{50} was calculated using the probit analysis method; B: Lysosomal membrane stability evaluated by the lysosomal enzyme β-glucuronidase activity in FVB and MT mice treated with or without LPS (4 mg/kg, i.p.) for 4 hrs. Mean ± SEM, n = 30 mice in each strain for panel A; n = 6–7 per group for panel B, p value provided in panel A exhibited significant difference between the two.

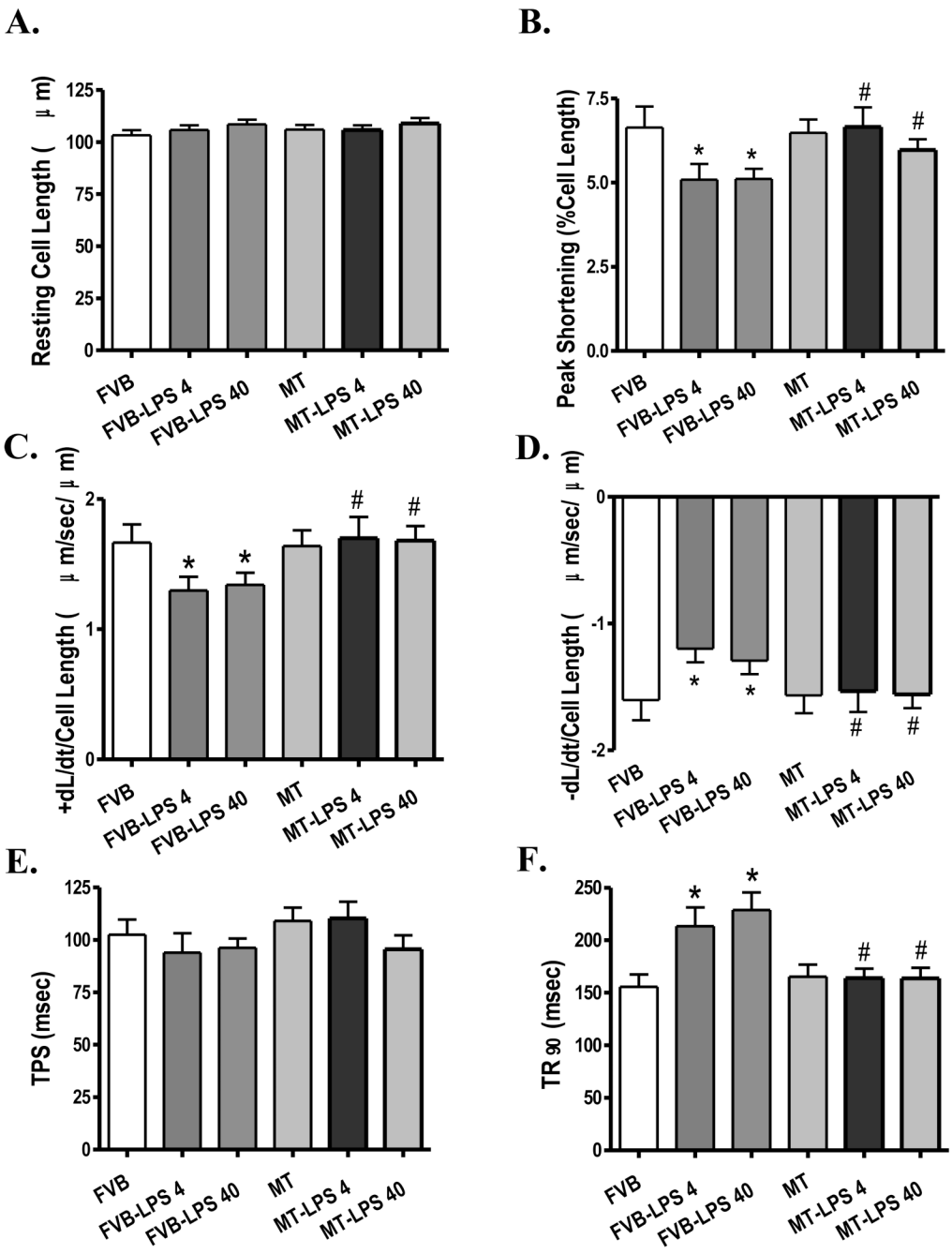

Fig. 2.

Cardiomyocyte contractile properties in FVB and MT transgenic mice treated with or without LPS (4 and 40 mg/kg, i.p.). A: Resting cell length; B: Peak shortening (PS, normalized to cell length); C: Maximal velocity of shortening (+ dL/dt); D: Maximal velocity of relengthening (− dL/dt); E: Time-to-PS (TPS); and F: Time-to-90% relengthening (TR_{90}). Mean ± SEM, n = 85–87 cells from 4 mice per group, * $p < 0.05$ *vs*. FVB group; # $p < 0.05$ *vs*. respective FVB-LPS group.

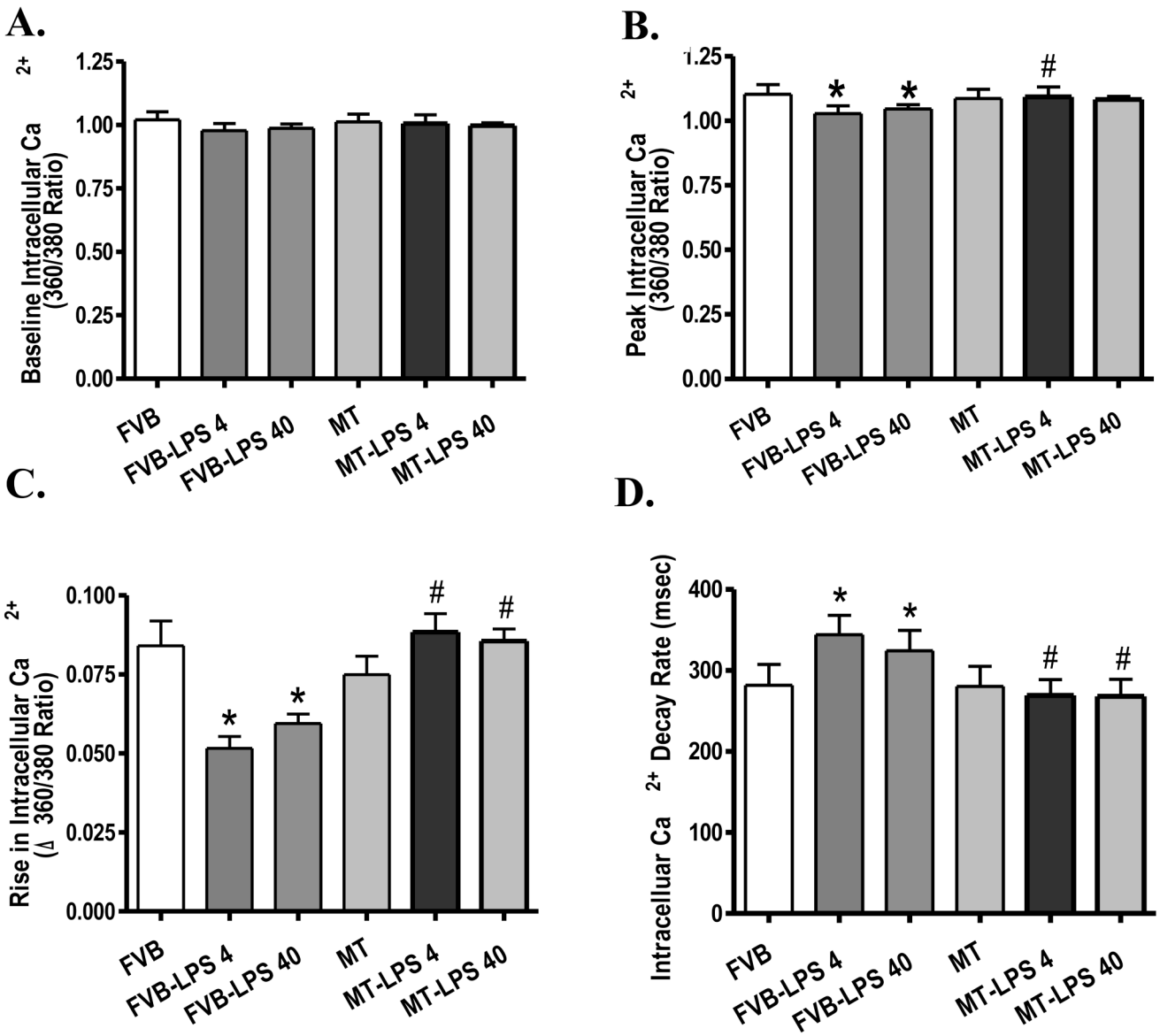

Fig. 3.

Intracellular Ca^{2+} properties in cardiomyocytes from FVB and MT mice treated with or without LPS (4 and 40 mg/kg, i.p.). A: Resting intracellular Ca^{2+}; B: Peak intracellular Ca^{2+}; C; Electrically-stimulated rise (peak – resting) in intracellular Ca^{2+}; and D: Intracellular Ca^{2+} decay rate. Mean ± SEM, n = 58–60 cells from 4 mice per group, * $p < 0.05$ *vs*. FVB group; # $p < 0.05$ *vs*. respective FVB-LPS group.

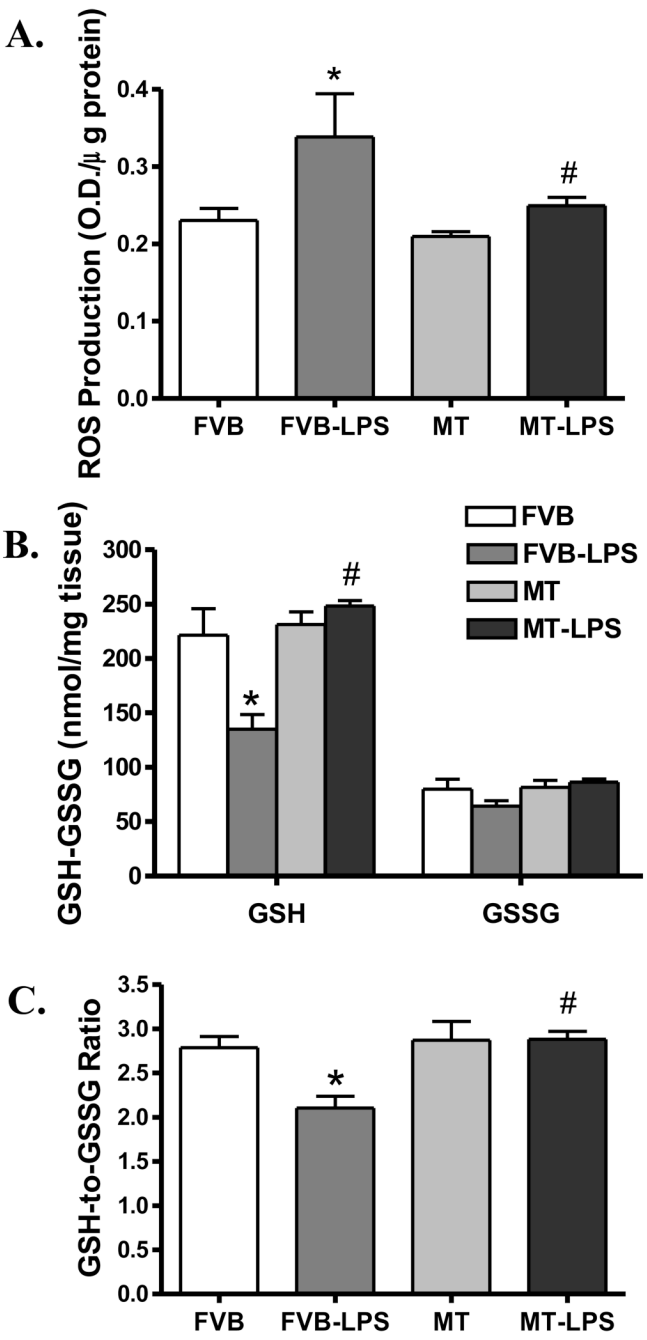

Fig. 4.

ROS production and oxidative stress in cardiomyocytes from FVB and MT transgenic mice treated with or without LPS (4 mg/kg, i.p.). A: ROS production measured by DCF fluorescence; B: Glutathione (GSH) and oxidized glutathione (GSSG) levels; and C: GSH/GSSG ratio. Mean ± SEM, n = 5 – 6 mice per group, * $p < 0.05$ *vs*. FVB; # $p < 0.05$ *vs*. FVB-LPS group.

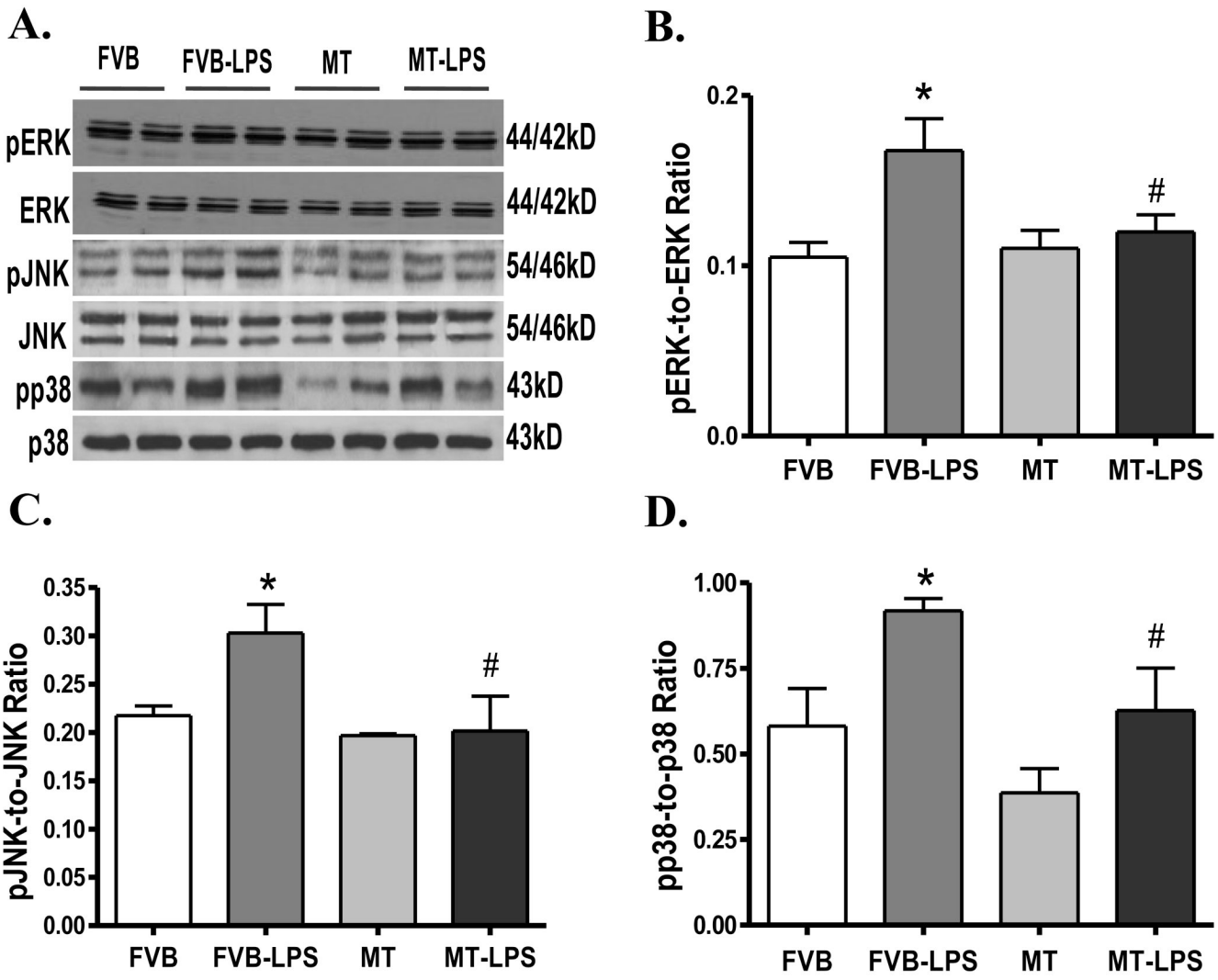

Fig. 5.

Western blot analysis exhibiting phosphorylation of ERK, JNK and p38 in myocardium from FVB and MT transgenic mice treated with or without LPS (4 mg/kg. i.p.). A: Representative gel blots depicting total and phosphorylated ERK, JNK and p38 proteins using specific antibodies; B: pERK-to-ERK ratio; C: pJNK-to-JNK ratio; and D: pp38-to-p38 ratio. Mean ± SEM, n = 4–6 samples per group, * $p < 0.05$ *vs*. FVB group, # $p < 0.05$ *vs*. FVB-LPS group.

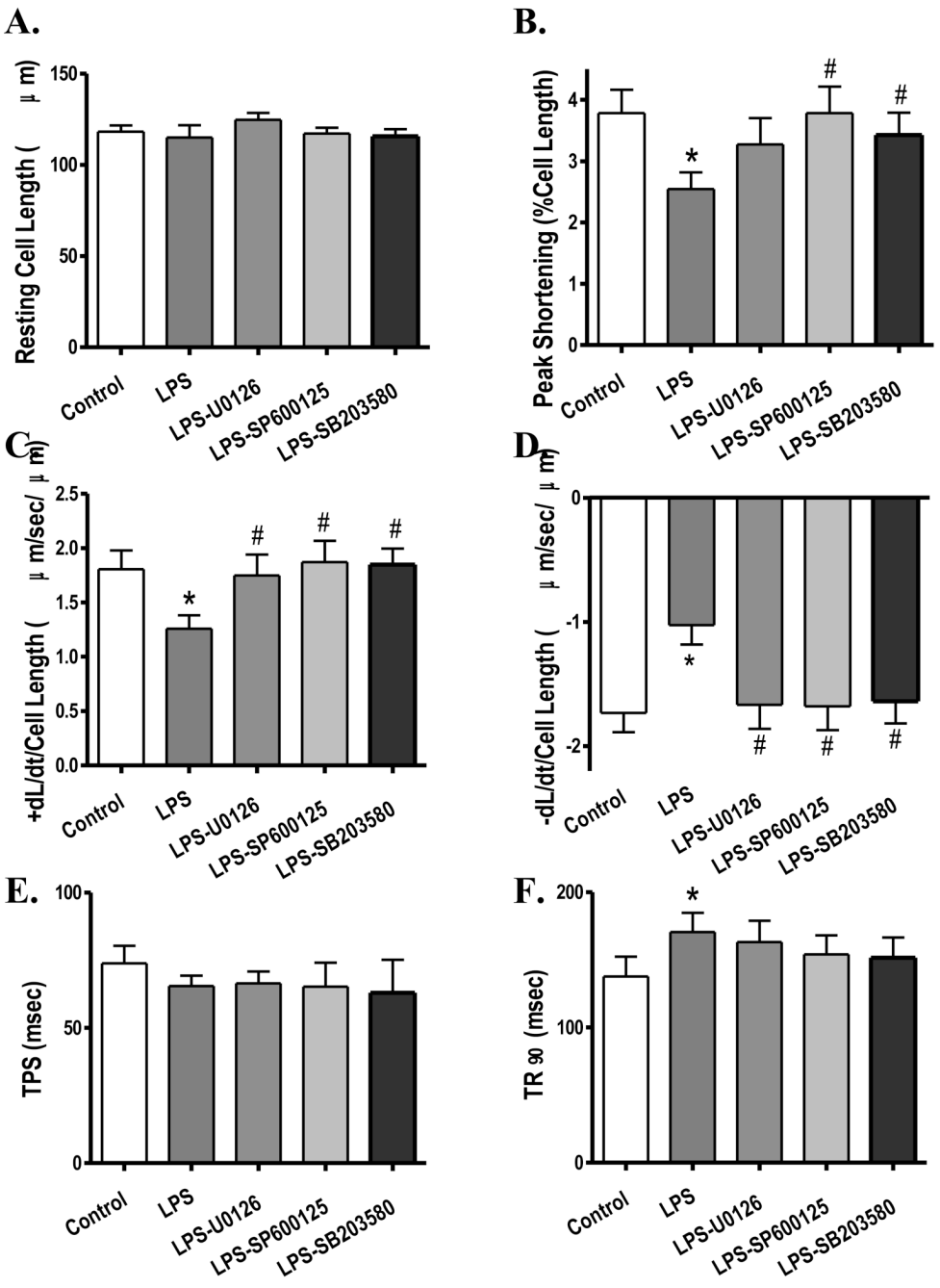

Fig. 6.

Effect of MPA kinase inhibition on LPS-induced cardiomyocyte contractile dysfunction. FVB (control) cardiomyocytes were incubated with LPS (4 μg/ml) at 37°C for 2 hrs in the absence or presence of the ERK inhibitor U0126 (1 μM), the JNK inhibitor SP600125 (1 μM) or the p38 MAPK inhibitor SB203580 (1 μM) prior to functional assessment. A: Resting cell length; B: Peak shortening (PS, normalized to cell length); C: Maximal velocity of shortening (+ dL/dt); D: Maximal velocity of relengthening (− dL/dt); E: Time-to-PS (TPS); and F: Time-to-90% relengthening (TR_{90}). Mean ± SEM, n = 52–54 cells from 3 mice per group, * $p < 0.05$ *vs.* control, # $p < 0.05$ *vs.* LPS group.

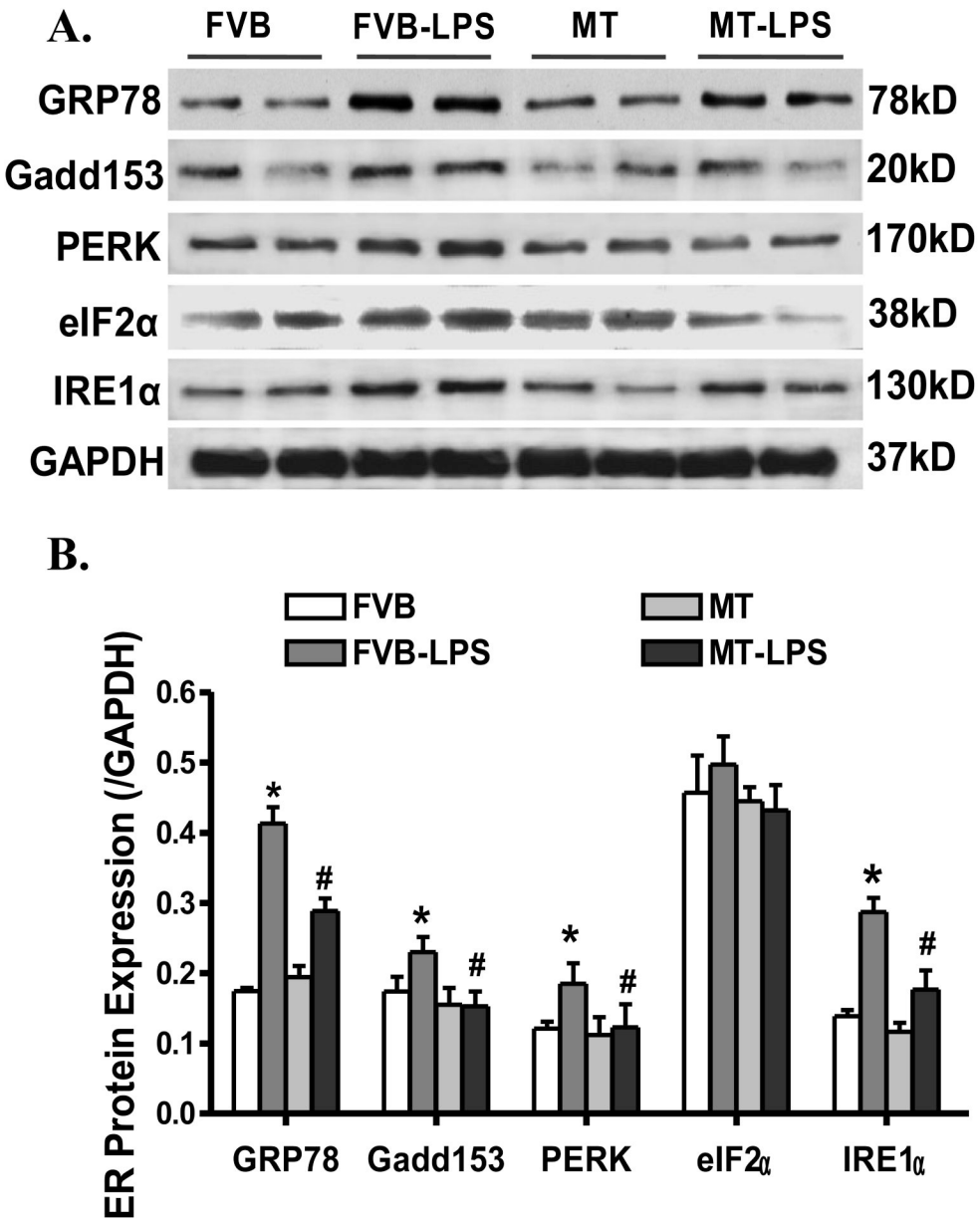

Fig. 7.

Western blot analysis displaying expression of the ER stress markers GRP78, Gadd153, PERK, eIF2α and IRE1α in myocardium from FVB and MT transgenic mice treated with or without LPS (4 mg/kg, i.p.). A: Representative gel blots depicting GRP78, Gadd153, PERK, eIF2α and IRE1α proteins using specific antibodies; B: Pooled data of GRP78, Gadd153, PERK, eIF2α and IRE1α proteins (normalized to GAPDH). Mean ± SEM, n = 3–6 samples per group, * $p < 0.05$ *vs*. FVB, # $p < 0.05$ *vs*. FVB-LPS group.

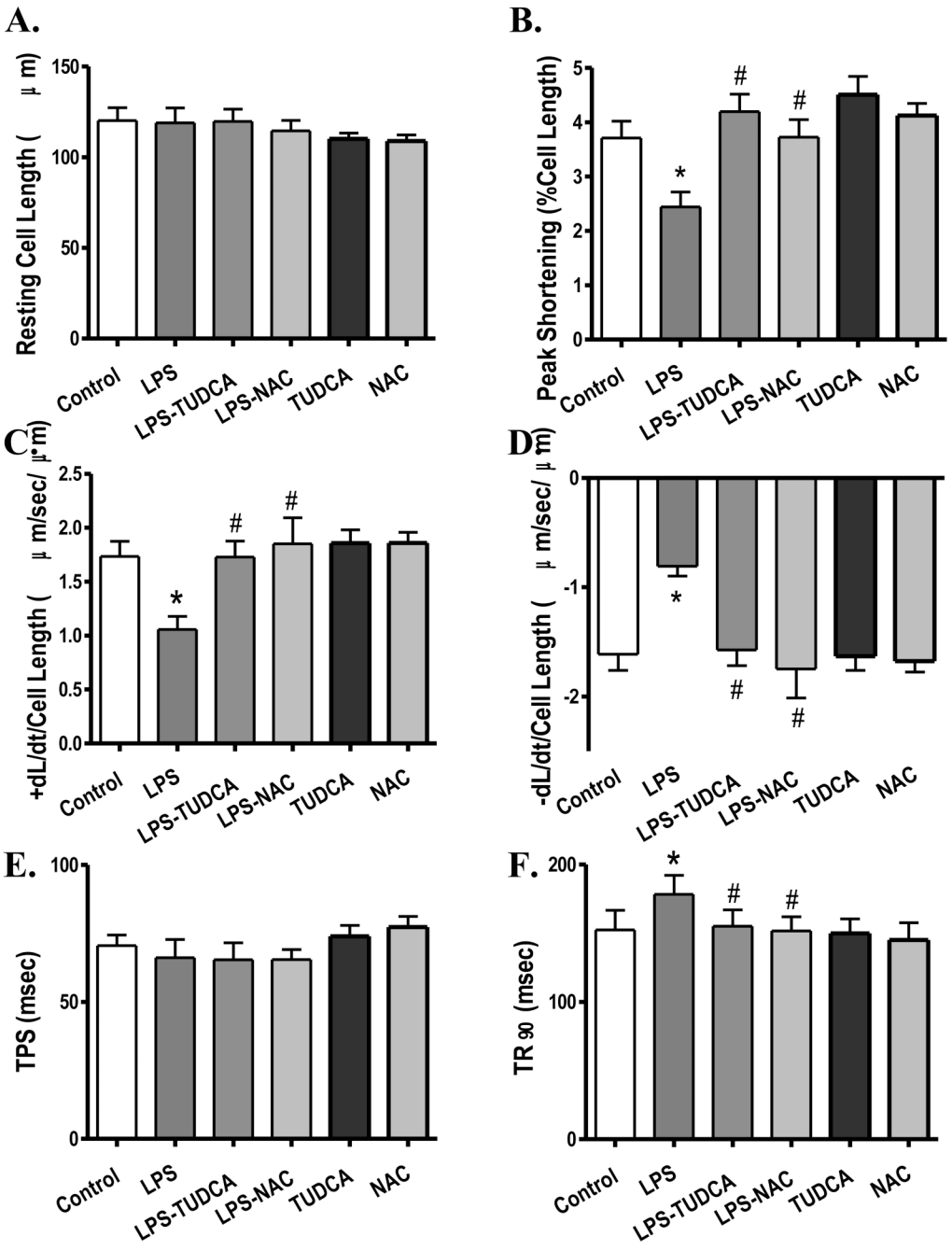

Fig. 8.

Effect of inhibition of ER stress and oxidative stress on LPS-induced cardiomyocyte contractile dysfunction. FVB (control) cardiomyocytes were incubated with LPS (4 μg/ml) at 37°C for 2 hrs in the absence or presence of the ER stress inhibitor tauroursodeoxycholic acid (TUDCA, 500 μM) or the antioxidant N-acetylcysteine (NAC, 500 μM) prior to mechanical assessment. A: Resting cell length; B: Peak shortening (PS, normalized to cell length); C: Maximal velocity of shortening (+ dL/dt); D: Maximal velocity of relengthening (− dL/dt); E: Time-to-PS (TPS); and F: Time-to-90% relengthening (TR_{90}). Mean ± SEM, n = 49–52 cells from 3 mice per group, * $p < 0.05$ *vs.* control, # $p < 0.05$ *vs.* LPS group.

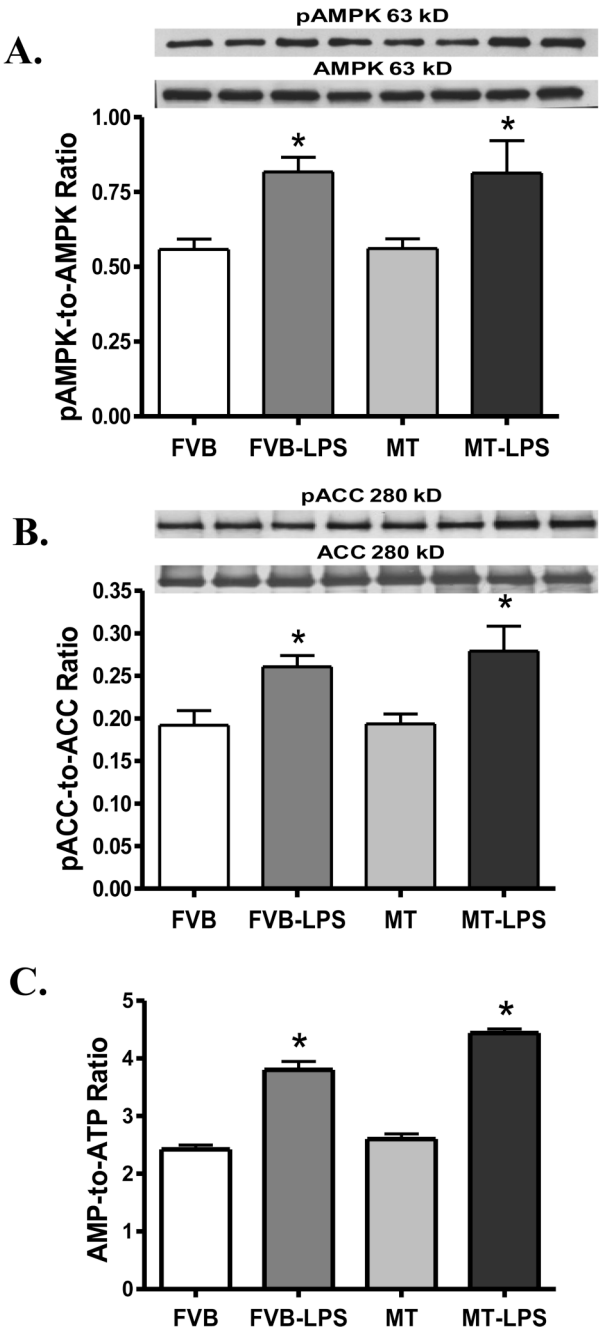

Fig. 9.

Expression of total and phosphorylated AMPK and ACC proteins as well as the AMP-to-ATP ratio in myocardium from FVB and MT transgenic mice treated with or without LPS (4 mg/kg, i.p.). A: pAMPK-to-AMPK ratio; B: pACC-to-ACC ratio; and C: AMP-to-ATP ratio. Mean ± SEM, n = 3–5 per group, * $p < 0.05$ *vs*. FVB, #$p < 0.05$ *vs*. FVB-LPS group.

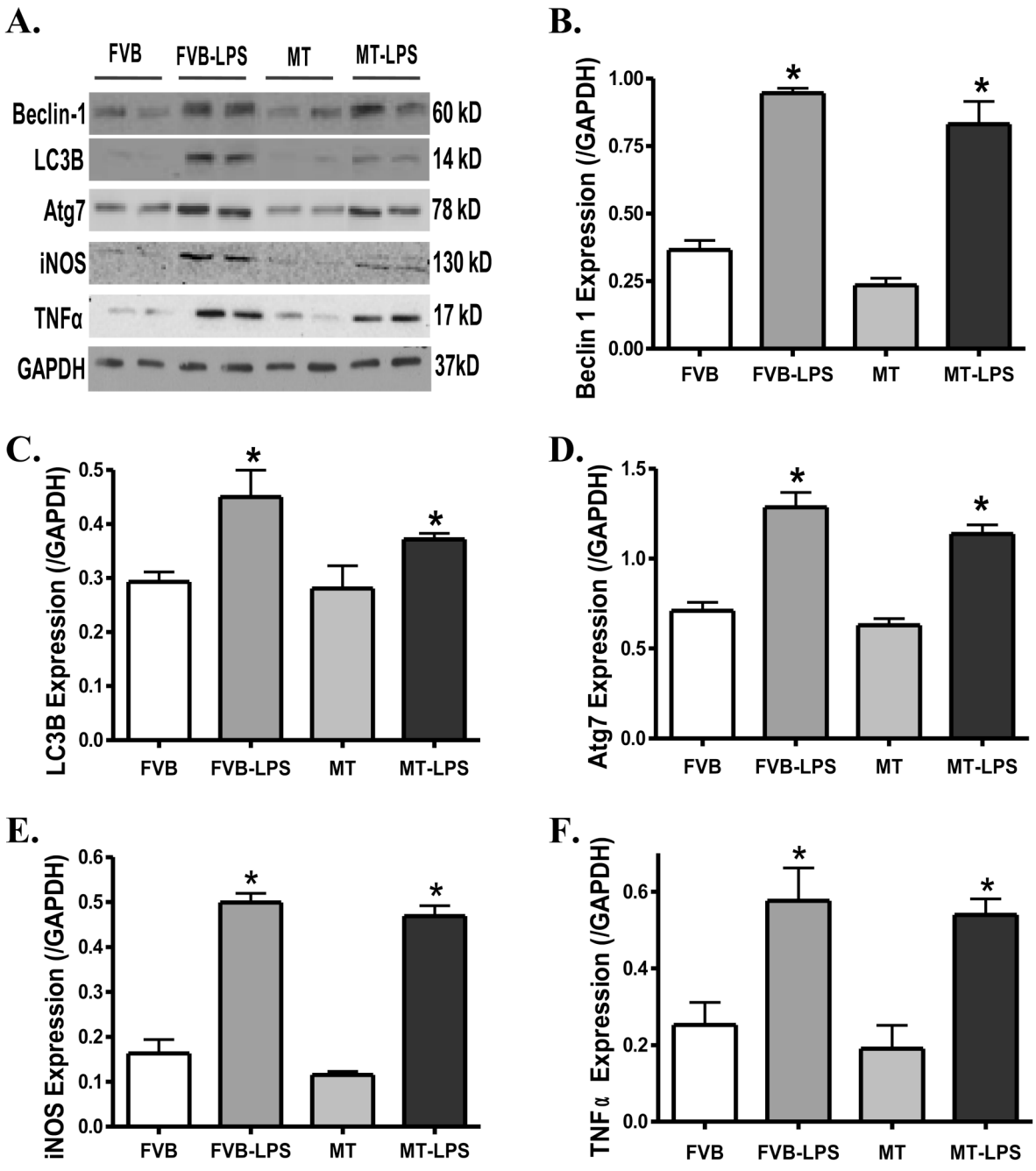

Fig. 10.

Protein expression of the autophagy markers Beclin-1, LC3B and Atg7 as well as the proinflammatory markers iNOS and TNFα in myocardium from FVB and MT mice treated with or without LPS (4 mg/kg, i.p.). A: Representative gel blots depicting Beclin-1, LC3B, Atg7, iNOS, TNFα and GAPDH (loading control) proteins using specific antibodies; B: Beclin 1; C: LC3B; D: Atg7; E: iNOS; and F: TNFα. Mean ± SEM, n = 3–4 per group, * $p < 0.05$ *vs*. FVB group.

Table 1

Biometric and echocardiographic parameters of LPS-treated FVB and MT mice

Parameter	FVB	FVB-LPS	MT	MT-LPS
Body Weight (g)	27.1 ± 1.0	27.9 ± 2.2	27.4 ± 1.0	27.8 ± 1.4
Heart Weight (mg)	138 ± 8	152 ± 19	147 ± 15	157 ± 8
Heart/Body Weight (mg/g)	4.87 ± 0.28	4.88 ± 0.18	4.57 ± 0.45	5.34 ± 0.17
Liver Weight (g)	1. 39 ± 0.10	1. 42 ± 0.20	1.28 ± 0.08	1.39 ± 0.07
Kidney Weight (g)	0.33 ± 0.02	0.34 ± 0.09	0.31 ± 0.01	0.30 ± 0.02
Heart Rate (bpm)	454 ± 24	455 ± 27	439 ± 41	445 ± 27
Wall Thickness (mm)	0.81 ± 0.04	0.79 ± 0.06	0.90 ± 0.09	0.82 ± 0.04
EDD (mm)	2.33 ± 0.17	2.16 ± 0.29	2.26 ± 0.23	2.14 ± 0.26
ESD (mm)	1.13 ± 0.14	1.44 ± 0.14*	1.20 ± 0.11	1.28 ± 0.09
LV Mass/Body Weight (mg/g)	2.07 ± 0.21	2.05 ± 0.30	2.34 ± 0.32	1.99 ± 0.41
Fractional Shortening (%)	51.8 ± 4.3	31.6 ± 3.8*	44.8 ± 2.9	46.8 ± 3.1#

EDD = end diastolic diameter; ESD = end systolic diameter; LV = left ventricular. Mean ± SEM, n = 8 – 10 mice per group,

* $p < 0.05$ *vs.* FVB group,

# $p < 0.05$ *vs.* FVB-LPS group